Passive microscopic fluidic diodes using asymmetric channels

Cite as: AIP Advances **9**, 085117 (2019); https://doi.org/10.1063/1.5115216
Submitted: 15 June 2019 • Accepted: 12 August 2019 • Published Online: 20 August 2019

Jingwen Mo, Yaohuan Ding, Shu Zhu, et al.

Passive microscopic fluidic diodes using asymmetric channels

Cite as: AIP Advances 9, 085117 (2019); doi: 10.1063/1.5115216
Submitted: 15 June 2019 • Accepted: 12 August 2019 •
Published Online: 20 August 2019

Jingwen Mo,[a] Yaohuan Ding, Shu Zhu, Pan Kuang, Long Shen, Nan Xiang,[b] Jingjie Sha, and Yunfei Chen[c]

AFFILIATIONS

Jiangsu Key Laboratory for Design & Manufacture of Micro/Nano Biomedical Instruments and School of Mechanical Engineering, Southeast University, Nanjing 210096, P.R. China

[a]Email: jwmo@seu.edu.cn
[b]Email: nan.xiang@seu.edu.cn
[c]Email: yunfeichen@seu.edu.cn

ABSTRACT

In this paper, we propose a passive microscopic fluidic diodes with no moving parts for simple fluids using asymmetric channel structures. Finite element simulations demonstrate that the fluidic diode conducts water flows preferentially in one forward direction while blocks flows in the reverse direction in a wide pressure range. The exceptional rectification performance is owing to the anisotropic direction-dependent activation pressures. In the forward direction, the activation pressure is small, which is controlled by the infiltration pressure of the small channel. In the backward direction, the activation pressure is large due to the high release pressure at the channel exit. The effective working pressure range for the fluidic diode can be flexibly adjusted by modifying the channel size or the surface property. Furthermore, we create a microfluidic diode fabricated on silicon membranes using laser direct writing. The diode achieves flow rectifications in a certain pressure range, which confirms the underlying rectification mechanisms. This work provides a novel strategy for flow control or logic computations in integrated micro- and nanofluidic systems.

INTRODUCTION

Microscopic fluidic logic elements are devices that can automatically regulate the fluid flow in programmed directions.[1–7] They play a critical role in large scale integration of microfluidic circuits, which require manipulation of minute amounts of fluid flow or biochemical reactions sequentially to realize various functionalities such as separation, synthesis, and detection.[8–12] In microfluidic systems, micro valves can function as the fluidic logic element.[10,13,14] However, they usually contain moving parts that need to be actuated by applying external pressure, heating, electrical or magnetic fields.[15] Scaling down the valves is difficult as it poses great challenges for fabrication and those moving parts may cause fatigue and reliability issues.[16] Passive fluidic logic elements (no moving parts) are generally preferred for fluid manipulation at small scales due to the high scalability.[17,18] Particularly, a basic unit of the fluidic logic elements is the fluidic diode, which rectifies the fluid to flow directionally. Since the fluid transport is different from the electron transport, it is challenging to completely block the fluid flow in one direction using fixed structures. Although a few passive fluidic diodes have been reported recently, extensive efforts are still needed to develop diverse small scale fluidic diodes to promote the applications of micro- and nanofluidic devices.[19,20]

In literature, most efforts were focused on the development of fluid rectifiers, which amplify the flow rates in a specified direction due to direction-dependent flow resistance.[21,22] Conventional fluidic rectifiers generally employ asymmetric structures such as the Tesla and nozzle-diffuser valves and can only achieve flow rectification at high Reynolds numbers or using non-Newtonian fluids.[23,24] The general problem with the fluidic rectifier is that the valving efficiency is poor, which results in flow leakage. In the past a few years, some biomimetic fluidic diodes have been demonstrated by introducing a wettability gradient to a surface using chemical, roughness, stiffness, or curvature gradient.[25–30] The unidirectional flow

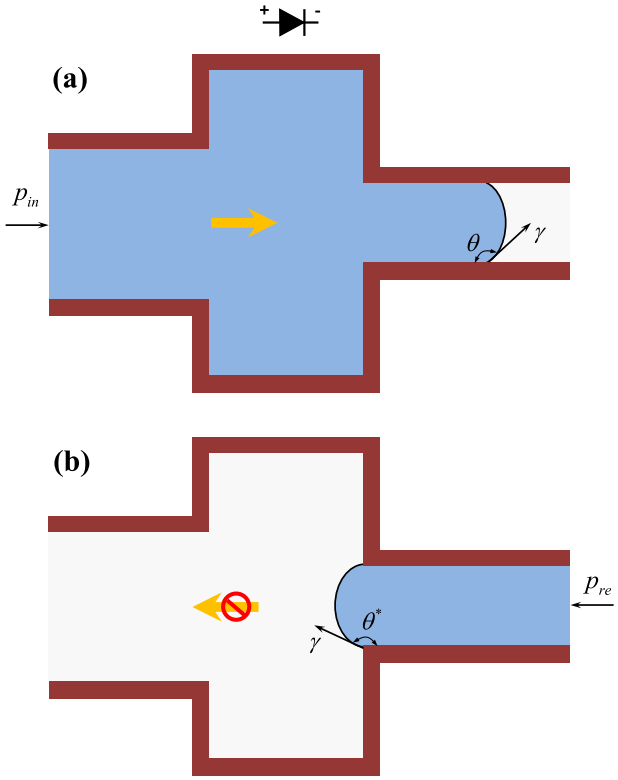

FIG. 1. Working principle of the fluidic diode. (a) To activate the flow, the pressure only needs to be higher than the infiltration pressure, p_{in}, of the small channel, (b) to break through the channel exit, the pressure has to be larger than p_{re} ($p_{re} > p_{in}$).

is achieved by the Laplace pressure difference generated around a droplet. For continuous flow, this directional transport capability may become weakened or lost. Another type of fluidic diodes utilizes porous membranes with heterogeneous surface wettability on the top and bottom sides to develop anisotropic flow resistance.[31–33] However, these diodes cannot be integrated into complex fluidic systems and their performances under high pressure is not clear. Recently, we propose three nanofluidic diodes for simple fluids using heterogeneous, nested, and non-uniform nanochannels.[34–36] In a wide range of pressure drops, flows in a specific direction are blocked due to either the entrance potential energy barrier arose from fluid-wall intermolecular interactions or the high release pressure caused by the small channel size.[37,38] Nonetheless, the development of passive fluidic diodes is still at the early stage and their applications in various areas such as logic computations require further explorations.

In this paper, we propose a microscopic diode for simple fluids using asymmetric channel structures. Finite element simulations show that water flows from the large channel to the small channel (forward direction) is allowed, while flows in the backward direction is prohibited in a wide pressure range. The blockage in the backward direction is owing to the increase in the contact angle, which raises the resistance due to surface tension, when water is released of the small channel, as illustrated in Fig. 1. This pressure range can be adjusted by modifying the channel size or the surface property for practical applications. A microfluidic device is fabricated, which realizes the diode function in a certain pressure range. Experiments confirm numerical observations and rectification mechanisms.

FINITE ELEMENT SIMULATION

A three dimensional finite element model using asymmetric microchannels was created in COMSOL and used to study the laminar flows. The asymmetric microchannel structure consists of two 200×160×500 μm (x×y×z) reservoirs connected by two 500×160 μm (x×y) microchannels and a 500×160×500 μm (x×y×z) junction as depicted in Fig. 2. To match the size and surface properties of manufactured fluidic chips used in experiments, the widths of the left and the right rectangular channels in the z direction are set to be w_l = 168 μm and w_r = 66 μm. The contact angles of water with the left/right and top/bottom channel walls are fixed as θ_{lr} = 120° and θ_{tb} = 100°. Initially, the reservoirs are filled with water while the microchannels are replete with air. The material properties such as density and dynamic viscosity of each region were directly imported from the built-in material library. The laminar two phase flow-phase field module in COMSOL was used. The pressure of the water reservoir is adjusted by applying an external pressure, P, at the leftmost or the rightmost boundary. For all simulations, transient solutions from 0 to 0.01 s were obtained. Simulation details can be found in the supplementary material.

FABRICATION OF MICROFLUIDIC DEVICE

The structure of the fluidic chip mimics the channel geometry used in numerical simulations, as demonstrated in Fig. 3(a). Noted the junction is mainly used to monitor the releasing process. The widths of the left and right channels (z direction) were 168±6 and 66±6 μm, measured from the microscopic image shown in Fig. 3(b). The size of all channels in the y direction was h = 160 μm. The

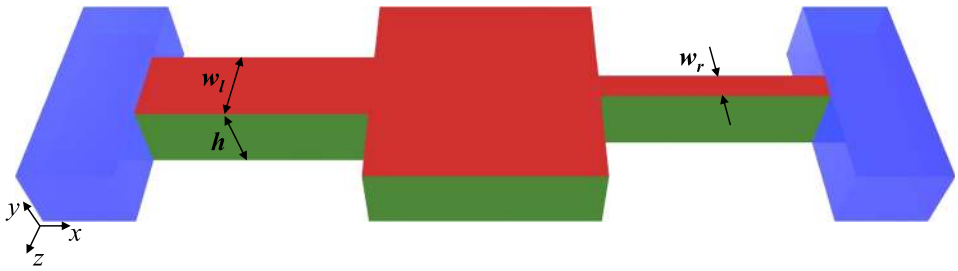

FIG. 2. The schematic of the COMSOL model.

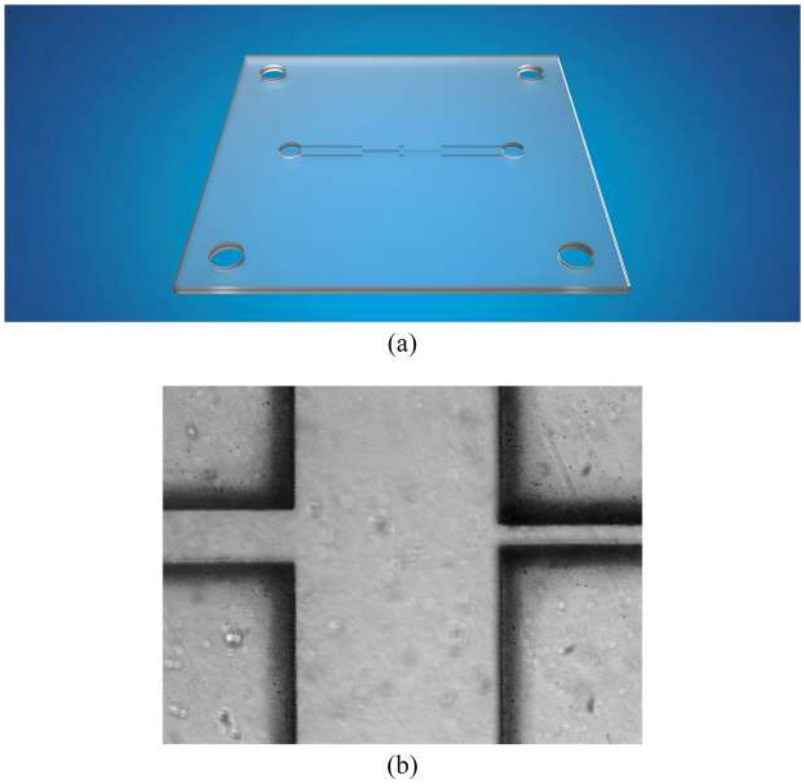

FIG. 3. (a) The microfluidic chip with the asymmetric channel structure, (b) microscopic image of microchannels at the chip center from the top view.

chip is fabricated using UV laser cut and plasma bonding method reported in our previous work.[39–41] Briefly, transparent silicon membranes with thickness of 160 μm were etched by a UV laser system (TH-UV200A, Tianhong Laser, China) to form the designed channel geometry, the inlet, the outlet and pin holes, as depicted in Fig. S1. To enhance the surface hydrophilicity, all membranes were exposed to plasma treatment for five minutes. After that, all layers were aligned and pressed to bond tightly. To connect and seal two reservoirs of the chip, a set of manufactured acrylic fixture was used to clamp the fluidic chip, as shown in Fig. 4.

The experimental setup is illustrated in Fig. 5. Compressed air was regulated by the pressure controller (OB1 Base MKIII,

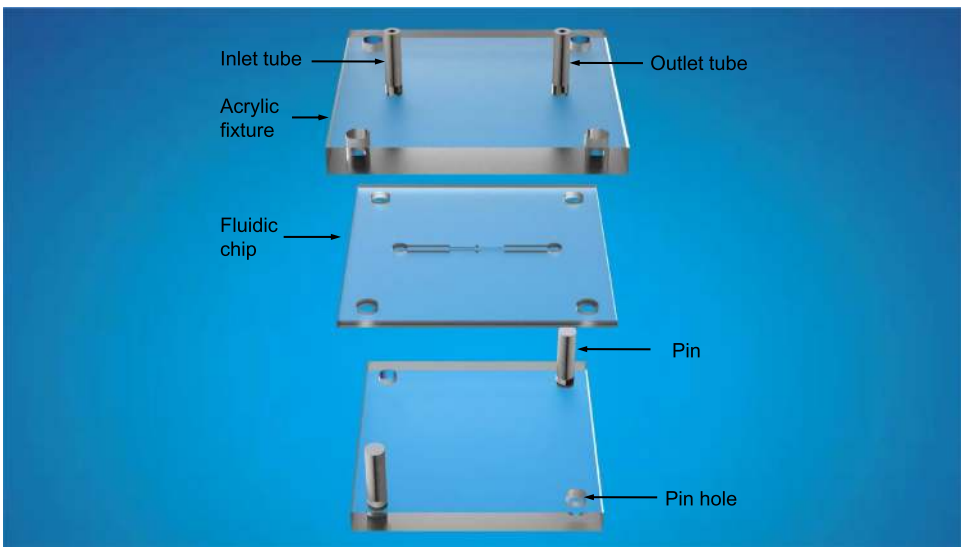

FIG. 4. Exploded drawing of the integrated microfluidic device.

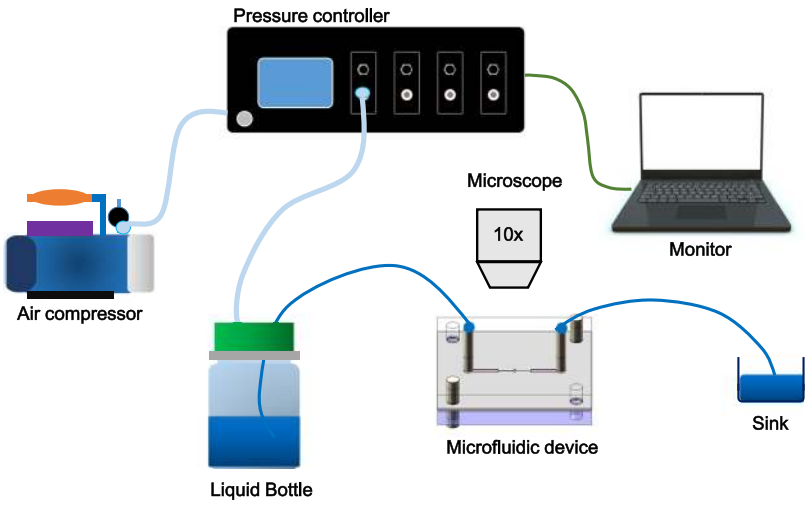

FIG. 5. Experimental setup of the fluidic system.

Elveflow) and was fed into a sealed liquid container (95% water and 5% carbon ink). The pressure controller was connected to a computer to adjust and measure the air pressure with an accuracy of 100 Pa. It is noted that the actual hydraulic pressure at the chip inlet, P_w, is calibrated from the relationship between the applied air pressure and the hydraulic head of water. The microfluidic device was fixed on the stage of an inverted fluorescent microscope (IX71, Olympus) equipped with a high-speed CCD camera (Retiga EXi, Qimaging). The motion of water flow inside microchannels was observed through an objective lens with 10x magnification. As the air pressure is gradually increased, water will be pushed into the fluidic chip. Initially, the two water reservoirs in the chip was filled with water. The activation pressures in the forward (left to right) or backward directions were determined by monitoring the hydraulic pressure, P_w, and the corresponding motion of the water meniscus.

RESULTS AND DISCUSSION

We first consider the finite element model with surface property and channel size approaching those of fabricated fluidic chips. The flow rectification of this system is studied by changing the applied pressure at the inlet P. Figure 6 demonstrates the flow rate as a function of the absolute driving pressure P in the forward (positive x) and the backward direction (negative x). It is seen that there are two critical pressures, $P_f^* \sim 1100$ Pa and $P_b^* \sim 2000$ Pa, which divides the flow behavior into three modes. When the pressure is low, $P < P_f^*$, water flows in both directions are not observed. When the pressure becomes higher than P_f^*, for $P_f^* < P < P_b^*$, water flows in the forward direction are turned on but still prohibited in the backward direction. In this pressure range, the asymmetric channel structure works as a fluidic diode that achieves unidirectional water flow. As P is increased further, $P > P_b^*$, flows in the backward direction is also activated. The flow rate in both directions tend to be the same and increase almost linearly with the driving pressure. This is similar to the breakdown of the diode. Noted the computed flow rate is verified using the Hagen-Poiseuille's equation for the pressure driven flow through rectangular channels with $w/h < 1$, where the pressure drop for the small channel is employed.[42]

The pressure range for this fluidic diode to be effective depends on P_f^* and P_b^*, which are the threshold pressures to activate the water flows. The difference between P_f^* and P_b^*, is caused by the distinct transport processes in each direction. In the forward direction, the conduction of water from the left reservoir to the right reservoir consists of three successive processes, i.e., the infiltration into the left channel, the water releasing, and then the wetting of the right channel, as illustrated in Fig. 7 (a)–(c). The theoretical capillary pressure for a rectangular microchannel can be calculated by the Young-Laplace equation, which is given by,[43]

$$p_c = -\gamma\left[\frac{2\cos\theta_{lr}}{w} + \frac{2\cos\theta_{tb}}{h}\right], \quad (1)$$

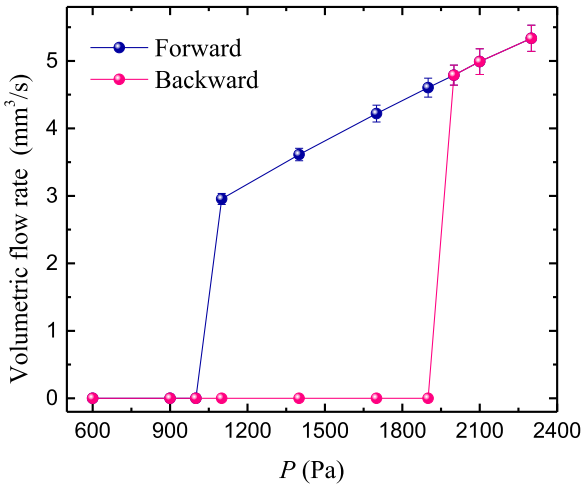

FIG. 6. Volumetric flow rate as a function of the driving pressure in the forward and backward directions obtained in simulations (w_l = 168 μm, w_r = 66 μm, θ_{lr} = 120°, and θ_{tb} = 100°).

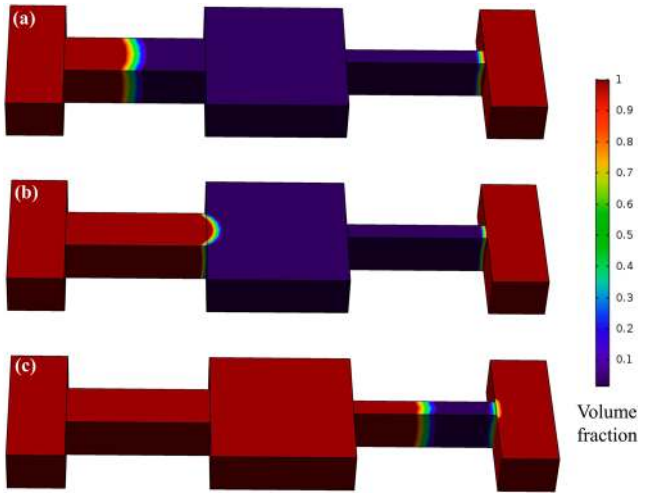

FIG. 7. Snapshots of the flow in the forward direction: (a) the infiltration of water into the left channel, P=600 Pa, (b) the meniscus shape before the breakthrough, P=780 Pa and (c) the wetting of the right channel, P=1100 Pa. The color bar represents the volume fraction of the water.

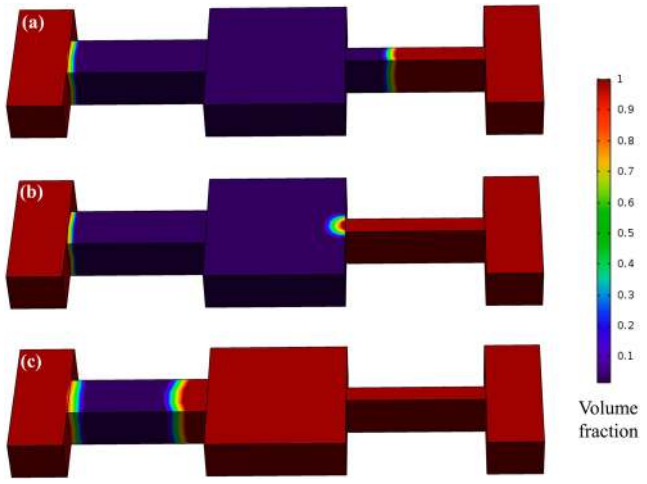

FIG. 8. Snapshots of the flow in the backward direction: (a) the filling of the right channel, P=1100 Pa, (b) the meniscus shape before the breakthrough, P=1900 Pa, (c) the wetting of the left channel. The color bar represents the volume fraction of the water.

where w is the channel width, h is the channel height, γ is the surface tension and θ_{lr}, θ_{tb} are contact angles of water with the left/right and top/bottom channel walls. Water must first infiltrate into the left channel. If water surface tension γ = 71.6 mN/m is used, the infiltration pressure for the left channel is estimated as p_{in} =~580 Pa. However, as water advances to the channel exit, the flow will be stopped due to the resistance caused by surface tension (Fig. 7(a)). As the pressure is gradually increased, the meniscus bulges outward and the contact angle increases which raises the resistance. When the pressure reaches the threshold, the effective contact angle achieves the highest (Fig. 7(b)). With a further slight increase in the pressure, water breaks through the exit. This critical pressure is defined as the release pressure, where the corresponding contact angle is termed as the largest effective contact angle. From Fig. 7(b), the largest effective contact angle is estimated to be θ_{lr} =~146° using the method in Refs. 35 and 44. If this angle is used in Eq. (1), the release pressure is predicted to be p_{re} =~860 Pa.[38] After releasing, the flow will still be blocked at the entrance of the right small channel since the channel width is narrowed by 2.5 times. The theoretical infiltration pressure of the right channel is computed to be ~1200 Pa, which is consistent with P_f^*. For flow in the backward direction, the transport of water from the right reservoir to the left reservoir also undergoes three consecutive stages, the filling of the right channel, the releasing from the channel, and then the wetting of the left channel, as illustrated in Fig. 8 (a)–(c). Still, a pressure of ~1200 Pa is needed to push water into the small channel. Analogously, the water flow will be blocked at the channel exit, which can be thought of as a more hydrophobic surface. To activate the releasing, the applied pressure should be larger than the release pressure. The largest effective contact angle is estimated to be ~148° from Fig. 8(b). The release pressure is predicted to be ~2000 Pa, which agrees with P_b^*. When the pressure is higher than P_b^*, the size of the droplet released out of the channel will grow continuously and the water front will advance into the left channel and finally merge with water in the left reservoir. Therefore, for the proposed asymmetric channel system, P_f^* and P_b^* are determined by the infiltration and the release pressure of the small channel respectively. If the pressure exceeds P_b^*, the infiltration and release pressures become insignificant and the flow rate in both directions are approximately the same. In this case, flow rectifications will not be observed unless the flow is at high Reynolds numbers (turbulence condition).[23]

Since the activation pressures is mainly dependent on the right small channel, their values can be varied by changing the size of the right channel. To find out the magnitude of effective pressure range of the fluidic diode that can be achieved, the channel width of the right channel is decreased from 66 μm to 200 nm. For computational convenience, we neglect the contribution of channel height to the capillary pressure, which is insignificant, and simplify the finite element model to a two dimensional one, as shown in the inset of Fig. 9. The contact angle of all channel walls are set to be 120° and the width of the left channel is still 168 μm. Figure 9 demonstrates the activation pressures P_f^* and P_b^* as a function of the channel width. It is seen that changing the channel width will simultaneously raise or reduce both P_f^* and P_b^*. The effective pressure range, $\Delta P = P_f^* - P_b^*$ increases as the channel width is decreased and assumes maximum, ~0.3 MPa at w = 200 nm. Noted that ΔP may increase further as w is reduced to nano- or molecular scale. In these regimes, atomic interactions become important and molecular dynamics simulations should be applied. It is worth mentioning that the simulation results of the release pressure are found to be consistent with the reported numerical and experimental data.[45,46]

To understand the effect of surface property on the activation pressures, we fix the contact angle of the left channel and the junction as θ = 120° while varying the contact angle of the right channel, θ_r. The widths of the left and right channels are set to be w_l = 168 μm and w_r = 20 μm respectively and other conditions remain the same as that of Fig. 9. Figure 10 demonstrates the activation pressures

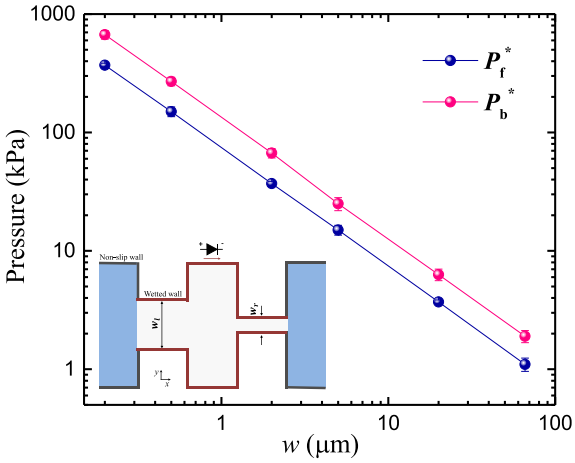

FIG. 9. Forward and backward activation pressures versus the width of the right channel (w_l = 168 μm, θ = 120°).

P_f^* and P_b^* versus the contact angle, θ_r. It is seen that as the surface is tuned hydrophilic ($50^\circ < \theta_r < 90^\circ$), P_f^* remains a constant, P_f^* = 700 Pa. This is because the infiltration pressure of the right channel is zero and P_f^* is controlled by the release pressure of the left channel. When the surface becomes hydrophobic ($\theta_r > 90^\circ$), P_f^* increases as θ_r is enlarged. In this regime, P_f^* depends on the infiltration pressure of the right channel, when it surpasses the release pressure of the left channel. It is found P_b^* increases monotonously with θ_r. The change in P_b^* is mainly due to the variations in the largest effective contact angle. The optimal surface property of the fluidic diode is at θ_r=~100°, where the pressure range for the system to be a diode assumes maximum.

Finally, to confirm the rectification mechanisms of the proposed fluidic diode, experiments are conducted to study water flow

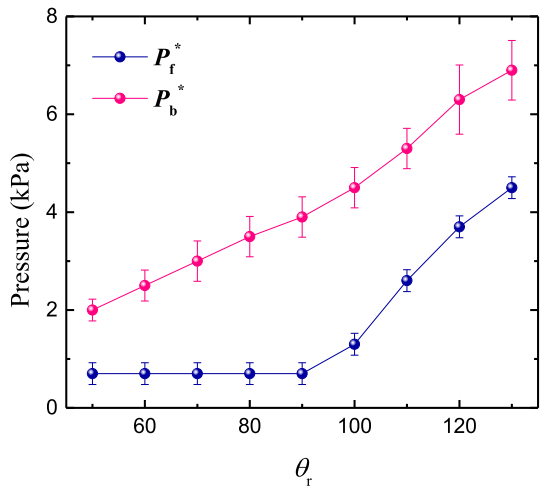

FIG. 10. Forward and backward activation pressures versus the contact angle of the right channel, θ_r (w_l = 168 μm, w_r = 20 μm).

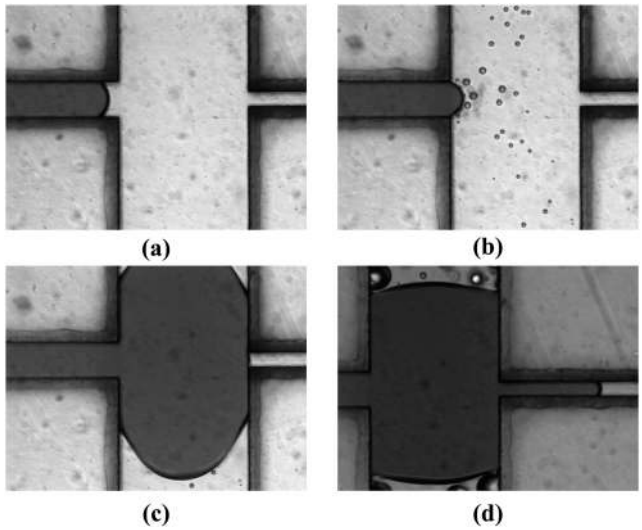

FIG. 11. Microscopic images illustrating the forward flow as a function of P_w: (a) the infiltration into the left channel, P_w=~470 Pa, (b) the blockage of flow at the exit, (c) the releasing from the channel, P_w=~700 Pa, and (d) flow into the right channel, P_w=~1320 Pa.

in microchannels. Figure 11 demonstrates the forward water flow as a function of P_w. It is seen that when P_w is increased to ~470±50 Pa, water will flow into the left channel and is stopped at the exit if P_w is not further enlarged (Fig. 11(a)). As P_w is increased, the meniscus shape becomes more curved and the effective contact angle increases (Fig. 11(b)). When P_w reaches ~700±50 Pa, water is released from the left channel to the junction, but is stuck at the entrance of the right channel (Fig. 11(c)). When P_w is higher than ~1320±70 Pa, water can be driven into the right channel and ultimately flows into the right reservoir (Fig. 11(d)). This critical pressure is the activation pressure in the forward direction, P_f^*. In the backward direction, similarly, a pressure of ~1320 Pa is required to drive water into the right channel (Fig. 12(a)). As P_w is increased, the contact angle grows to resist water from releasing and reaches the highest when P_w =~ 1890 ± 70 Pa (Fig. 12(b)). When P_w is slightly increased, water quickly break through the rest channels and flow into the left reservoir. Therefore, the fabricated microfluidic system can act as a fluidic diode in this pressure range, $1320 < P_w < 1890$ Pa, which is consistent with theoretical results.

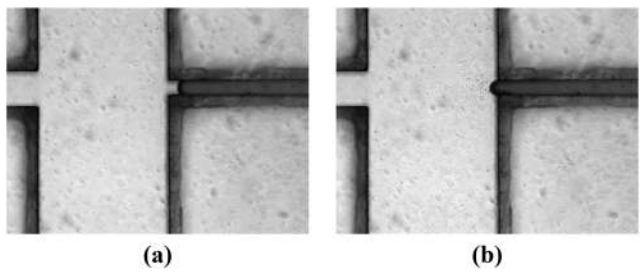

FIG. 12. Microscopic images demonstrating water meniscus shape for flow into (a) the right channel, P_w=~1320 Pa, (b) the junction, P_w=~1890 Pa.

CONCLUSION

In summary, we have demonstrated an asymmetric channel structure to act as a fluidic diode in a wide pressure range. Flow rectifications are guaranteed by direction-dependent activation pressures, which are caused by distinct flow mechanisms in the forward and backward directions. The effective working pressure range for the fluidic diode can be flexibly tuned for practical applications by varying the channel size or the surface property. A microfluidic diode is fabricated, which is effective over a certain pressure range. Experiments confirm the explanation about anisotropic activation pressures due to differences in the infiltration and release pressures.

SUPPLEMENTARY MATERIAL

See supplementary material for the detailed information about finite element simulations and the fluidic device.

ACKNOWLEDGMENTS

This work was supported by the National Natural Science Foundation of China under Grant No. (51805082, 51435003, 51875103) and the Natural Science Foundation of Jiangsu Province under Grant No. BK20170683.

REFERENCES

[1] M. Zhang, L. Wang, X. Wang, J. Wu, J. Li, X. Gong, J. Qin, W. Li, and W. Wen, Soft Matter **7**, 7493 (2011).
[2] G. Katsikis, J. S. Cybulski, and M. Prakash, Nat. Phys. **11**, 588 (2015).
[3] L. F. Cheow, L. Yobas, and D.-L. Kwong, Appl. Phys. Lett. **90**, 054107 (2007).
[4] M. Rhee and M. A. Burns, Lab Chip **9**, 3131 (2009).
[5] M. W. Toepke, V. V. Abhyankar, and D. J. Beebe, Lab Chip **7**, 1449 (2007).
[6] M. Prakash and N. Gershenfeld, Science **315**, 832 (2007).
[7] A. Groisman, M. Enzelberger, and S. R. Quake, Science **300**, 955 (2003).
[8] M. L. Kovarik, P. C. Gach, D. M. Ornoff, Y. Wang, J. Balowski, L. Farrag, and N. L. Allbritton, Anal. Chem. **84**, 516 (2012).
[9] M. L. Kovarik, D. M. Ornoff, A. T. Melvin, N. C. Dobes, Y. Wang, A. J. Dickinson, P. C. Gach, P. K. Shah, and N. L. Allbritton, Anal. Chem. **85**, 451 (2013).
[10] T. Thorsen, S. J. Maerkl, and S. R. Quake, Science **298**, 580 (2002).
[11] D. Mark, S. Haeberle, G. Roth, F. von Stetten, and R. Zengerle, Chem. Soc. Rev. **39**, 1153 (2010).
[12] J. Kolaas, A. Jensen, and M. Mielnik, Eur. Phys. J. E **36**, 19 (2013).
[13] M. A. Unger, H.-P. Chou, T. Thorsen, A. Scherer, and S. R. Quake, Science **288**, 113 (2000).
[14] B. Mosadegh, C.-H. Kuo, Y.-C. Tung, Y.-s. Torisawa, T. Bersano-Begey, H. Tavana, and S. Takayama, Nat. Phys. **6**, 433 (2010).
[15] K. W. Oh and C. H. Ahn, J. Micromech. Microeng. **16**, R13 (2006).
[16] W. S. N. Trimmer, Sens. Actuator. **19**, 267 (1989).
[17] J. W. Hong and S. R. Quake, Nat. Biotechnol. **21**, 1179 (2003).
[18] E. Delamarche, D. Juncker, and H. Schmid, Adv. Mater. **17**, 2911 (2005).
[19] G. M. Whitesides, Nature **442**, 368 (2006).
[20] J. Melin and S. R. Quake, Annu. Rev. Biophys. Biomolec. Struct. **36**, 213 (2007).
[21] M. Nabavi, Microfluid. Nanofluid. **7**, 599 (2009).
[22] A. Olsson, G. Stemme, and E. Stemme, Sens. Actuator A-Phys. **47**, 549 (1995).
[23] P. C. Sousa, F. T. Pinho, M. S. N. Oliveira, and M. A. Alves, J. Non-Newton. Fluid Mech. **165**, 652 (2010).
[24] A. Groisman and S. R. Quake, Phys. Rev. Lett. **92**, 094501 (2004).
[25] J. Li, Y. Song, H. Zheng, S. Feng, W. Xu, and Z. Wang, Soft Matter **15**, 1902 (2019).
[26] J. Li, X. Zhou, J. Li, L. Che, J. Yao, G. McHale, M. K. Chaudhury, and Z. Wang, Sci. Adv. **3**, eaao3530 (2017).
[27] J. Ju, H. Bai, Y. Zheng, T. Zhao, R. Fang, and L. Jiang, Nat. Commun. **3**, 1247 (2012).
[28] P. Comanns, G. Buchberger, A. Buchsbaum, R. Baumgartner, A. Kogler, S. Bauer, and W. Baumgartner, J. R. Soc. Interface **12**, 20150415 (2015).
[29] Y. Si, T. Wang, C. Li, C. Yu, N. Li, C. Gao, Z. Dong, and L. Jiang, ACS Nano **12**, 9214 (2018).
[30] K.-H. Chu, R. Xiao, and E. N. Wang, Nat. Mater. **9**, 413 (2010).
[31] Y. Zhao, H. Wang, H. Zhou, and T. Lin, Small **13**, 1601070 (2017).
[32] J. E. Mates, T. M. Schutzius, J. Qin, D. E. Waldroup, and C. M. Megaridis, ACS Appl. Mater. Interfaces **6**, 12837 (2014).
[33] H. Chen, J. Cogswell, C. Anagnostopoulos, and M. Faghri, Lab Chip **12**, 2909 (2012).
[34] L. Li, J. Mo, and Z. Li, Phys. Rev. Lett. **115**, 134503 (2015).
[35] J. Mo, L. Li, J. Wang, and Z. Li, Phys. Rev. E **93**, 033101 (2016).
[36] J. Mo, C. Li, L. Li, J. Wang, and Z. Li, Phys. Fluids **28**, 082005 (2016).
[37] J. Mo, L. Li, J. Zhou, D. Xu, B. Huang, and Z. Li, Phys. Rev. E **91**, 033022 (2015).
[38] J. Mo, J. Sha, D. Li, Z. Li, and Y. Chen, Nanoscale **11**, 8408 (2019).
[39] X. Zhang, D. Huang, W. Tang, D. Jiang, K. Chen, H. Yi, N. Xiang, and Z. Ni, RSC Adv. **6**, 9734 (2016).
[40] X. Zhang, Z. Zhu, N. Xiang, F. Long, and Z. Ni, Anal. Chem. **90**, 4212 (2018).
[41] X. Zhang, Z. Zhu, Z. Ni, N. Xiang, and H. Yi, Biomed. Microdevices **19**, 21 (2017).
[42] M. Fuerstman, A. Lai, M. Thurlow, S. Shevkoplyas, H. Stone, and G. Whitesides, Lab Chip **7**, 1479 (2007).
[43] E. Delamarche, A. Bernard, H. Schmid, A. Bietsch, B. Michel, and H. Biebuyck, J. Am. Chem. Soc. **120**, 500 (1998).
[44] Solved with COMSOLMultiphysics 5.0, Filling of a capillary Channel: Level Set and Phase Field Models.
[45] K. Kistrup, C. E. Poulsen, P. F. Østergaard, K. B. Haugshøj, R. Taboryski, A. Wolff, and M. F. Hansen, J. Micromech. Microeng. **24**, 125007 (2014).
[46] H. Cho, H.-Y. Kim, J. Y. Kang, and T. S. Kim, J. Colloid Interface Sci. **306**, 379 (2007).